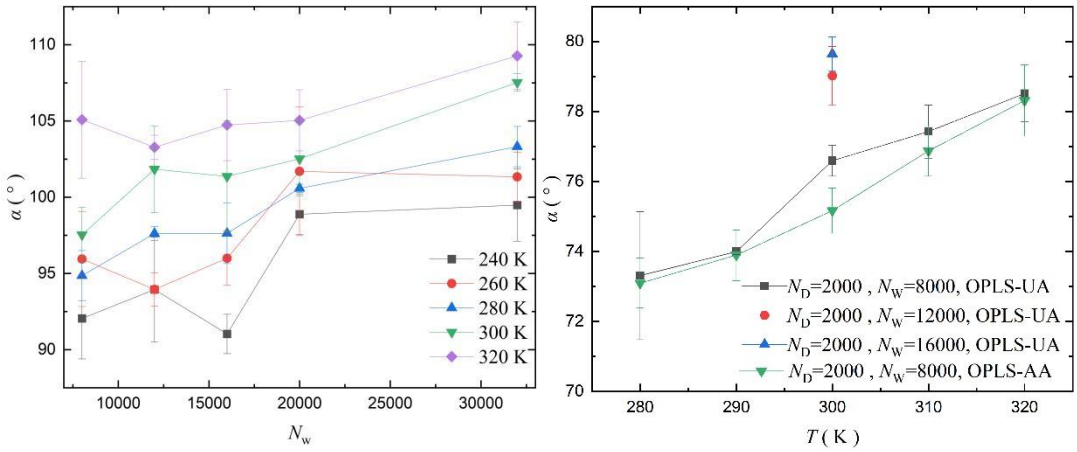
Reviewer 2

This is a thorough review of the manuscript titled: "Molecular dynamics study on the liquid-liquid contact angle in liquid-liquid phase separated aerosol". I suggest Major revision due to the following reasons:

1. **The manuscript compares Martini and OPLS-UA, but it never clearly explains:**

- **Which force field is expected to be more reliable for the present systems?**
- **Which one should readers trust when the two produce noticeably different contact angles and different NaCl aggregation behavior?**
- **Are these differences due to coarse-graining, parameterization, or some other physical reason?**

Answer: Thank you very much for this valuable comment. In order to evaluate the accuracy of the Martini and OPLS-UA force field parameters, the contact angles of binary water (N_W = 8000)-dodecane (N_D = 2000) droplets at difference temperatures based on the OPLS-AA all-atom force field are calculated. The comparison of the calculation results of three force field parameters is shown in Fig. 3.



(a) (b)

Fig. 3. Contact angles of water-dodecane droplets under different temperature and water content conditions. (a) Results of the Martini force field (N_D = 2000), and (b) results of the OPLS-UA and the OPLS-AA force field

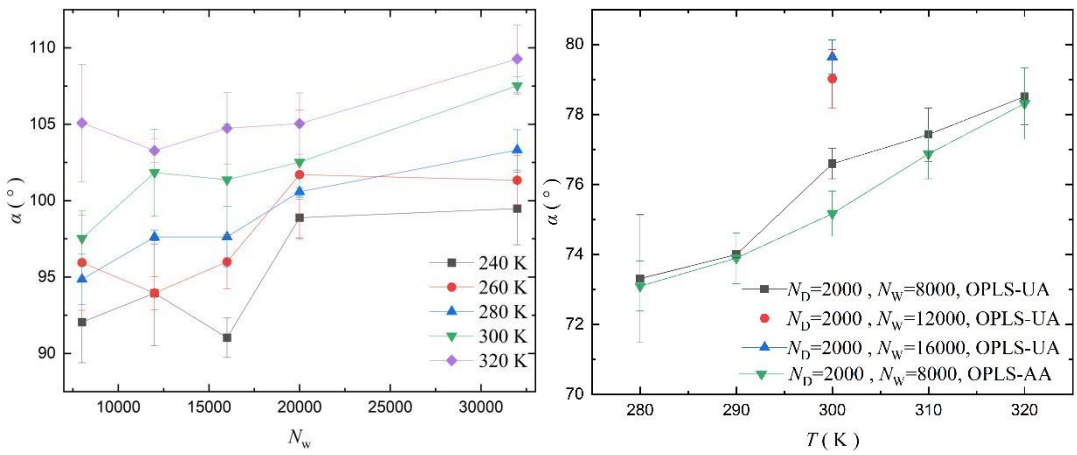
It can be observed from Fig. 3(b) that the contact values calculated by the OPLS-AA force filed are in good agreement with those from the OPLS-UA force field.

However, results of the Martini force field are significantly greater than those of the UA force field. Therefore, OPLS-UA force field is more reliable for the present systems. Meanwhile, the contact angle and NaCl aggregation behavior based on the OPLS-UA force field is expected to be more reliable.

The Martini force field parameters have limitations in describing the surface tension of pure water and therefore the water-dodecane contact angle. The core problem of the Martini force field lies in the compromises inherent in its coarse-grained design: representing multiple water molecules with a single bead eliminates orientational degrees of freedom and hydrogen-bond directionality, yet water's surface tension arises precisely from the anisotropic net attraction caused by surface molecules being unable to form a complete hydrogen-bonding network. Meanwhile, in Martini force filed each water bead is modeled as a simple 12-6 Lennard-Jones particle, and its nonbonded parameters are optimized for bulk-phase partitioning free energies. Because such a simplified LJ potential is known to overly stabilize the solid phase and cause unphysical freezing at elevated temperatures, the force field deliberately avoids using surface tension as a fitting target. Consequently, its water beads lack explicit hydrogen bonding and electrostatics, causing the predicted surface tension of pure water to be only about one-third of the experimental value (Iannetti et al., 2024).

In the revised manuscript, the discussion on the MD results based on OPLS-AA force field parameters and the limitations of Martini force field parameters has been added, as shown below.

To evaluate the accuracy of the Martini force field and the OPLS-UA force field parameters, the contact angles of binary water (N_w = 8000)-dodecane (N_D = 2000) droplets at difference temperatures based on the OPLS-AA all-atom force field (Jorgensen et al., 1996) are also presented.



(a) (b)

Fig. 3. Contact angles of water-dodecane droplets under different temperature and water content conditions. (a) Results of the Martini force field (N_D = 2000), and (b) results of the OPLS-UA force field and the OPLS-AA force field

As shown in Fig. 3(a), when the temperature is constant, the contact angle is positively correlated with the number of water molecules, which is consistent with the qualitative results obtained from Fig. 2. In addition, when the content of water molecules in the droplet is the same, the contact angle shows an increasing trend with the increase of temperature. This result is consistent with the variation of the contact angle between nonane and water with temperature in Obeidat et al. (2015). It can be seen from Fig. 3(b) that the contact angle obtained based on the OPLS-UA force field is positively correlated with both temperature and water molecule content, which is consistent with the result based on the Martini force field. The mechanism of temperature's effect on contact angle will be discussed in the Discussions section (Section 3.5), taking into account the results of changes in interfacial tension. Fig. 3(b) also indicates that the contact values calculated by the OPLS-AA force filed are in good agreement with those from the OPLS-UA force field. However, results of the Martini force field are significantly greater than those of the UA force field.

(shown in lines 221 ~ 244 , pages 11-13 in the revised manuscript)

The Martini force field parameters have limitations in describing the surface tension of pure water and therefore the water-dodecane contact angle. The core problem of the Martini force field lies in the compromises inherent in its coarse-grained design:

representing multiple water molecules with a single bead eliminates orientational degrees of freedom and hydrogen-bond directionality, yet water's surface tension arises precisely from the anisotropic net attraction caused by surface molecules being unable to form a complete hydrogen-bonding network. Meanwhile, in Martini force field each water bead is modeled as a simple 12-6 Lennard-Jones particle, and its nonbonded parameters are optimized for bulk-phase partitioning free energies. Because such a simplified LJ potential is known to overly stabilize the solid phase and cause unphysical freezing at elevated temperatures, the force field deliberately avoids using surface tension as a fitting target. Consequently, its water beads lack explicit hydrogen bonding and electrostatics, causing the predicted surface tension of pure water to be only about one-third of the experimental value (Iannetti et al., 2024). Nevertheless, despite these limitations in quantitatively reproducing interfacial properties, The Martini force field remains a highly efficient coarse-grained model, valuable for investigating qualitative mechanisms underlying how microscopic parameters modulate interfacial behavior, especially for exploring particle size effects.

(shown in lines 601 ~ 618 , page 34 in the revised manuscript)

2. **Are there any experimental measurements or previous MD simulations that can quantitatively validate the predicted contact angles, rather than only the interfacial tensions?**

Answer: Thank you very much for this valuable comment. To date, no quantitative experimental measurements or prior molecular dynamics (MD) simulation data of liquid-liquid contact angles for nanoscale LLPS dodecane-water aerosol droplets have been reported in existing literature, which is explicitly acknowledged and discussed in our manuscript.

Only interfacial tension data from experiments and previous MD works are available for cross verification, which we have fully compared and validated in Section 3.4 and Figure 8 of this paper to verify the reliability of our two force field frameworks (Martini and OPLS-UA).

In the revised manuscript, we have added molecular simulations based on the OPLS-AA force field to verify the reliability of the Martini and OPLS-UA force fields (Figure 3).

For future research, we plan to conduct systematic quantitative contact angle measurements on LLPS aerosol particles via environmental scanning electron microscopy (ESEM) and single-beam optical trap (aerosol optical tweezers). These experimental platforms can capture nanoscale phase-separated droplet morphology and extract liquid-liquid contact angles quantitatively, which will enable direct quantitative validation of our MD-predicted contact angles in follow-up studies.

3. **How representative is dodecane of real atmospheric organic aerosols? Would the conclusions remain valid for more oxygenated organic compounds?**

Answer: Thank you very much for this valuable comment. It should be noted that dodecane is adopted as a simplified surrogate for low-oxygen nonpolar aliphatic organics in atmospheric aerosols, which cannot fully represent highly oxygenated organic compounds abundant in ambient particles. Nevertheless, the core qualitative conclusions of this study, derived from universal interfacial tension competition thermodynamics, remain valid for general water-organic LLPS aerosol systems: contact angle positively correlates with temperature and water loading, while negatively correlates with inorganic salt and surfactant concentrations; classical Young's equation cannot accurately predict nanoscale contact angles without line tension correction. For highly oxygenated organics with elevated O:C ratios, stronger water-organic hydrogen bonding will reduce water-organic interfacial tension and yield smaller equilibrium liquid-liquid contact angles compared to dodecane systems. In future work, we will perform systematic MD simulations on organics with gradient oxygenation degrees and diverse functional groups to quantify the influence of organic oxygenation on LLPS contact angles and further verify the generalizability of the proposed thermodynamic mechanisms.

4. **Why was suberic acid chosen instead of more common atmospheric organic acids**

such as oleic acid or succinic acid?

Answer: Thank you very much for this valuable comment. In this study, suberic acid (C8 linear dicarboxylic acid) was selected as the representative amphiphilic organic acid rather than succinic acid or oleic acid, for the following reasons.

From the perspective of force field parameters, suberic acid is the smallest dicarboxylic acid molecule that can be coarsened by Martini's force field. If the number of carbon atoms decreases, the coarsening force field cannot be used. If the number of carbon atoms is too large, the computational workload will increase.

From the perspective of component properties, short-chain dicarboxylic acids exhibit extremely high aqueous solubility. They scarcely accumulate at the water–organic interface, and thus fail to induce appreciable reductions in interfacial tension or measurable variations in contact angle. Suberic acid has balanced amphiphilicity with a medium-length C8 alkyl chain and two terminal carboxyl groups, which enables obvious enrichment at the water-dodecane interface and produces a concentration-dependent reduction in liquid-liquid contact angle that can be quantitatively analyzed.

Future work will systematically compare dicarboxylic acids with different carbon chain lengths and monocarboxylic unsaturated acids to further generalize the influence of organic acid structure on LLPS contact angles. The revisions incorporated in the revised manuscript are listed below.

It should be acknowledged that our model systems are simplified compared to real multi-organic multi-salt atmospheric aerosols. All simulated LLPS droplets are smaller than 20 nm, representative of fresh nucleation mode ultrafine particles from new particle formation and fuel combustion. Though these nanoparticles dominate ambient aerosol number concentrations and govern early aging processes, our results cannot be directly extrapolated to larger aged accumulation mode aerosols. Future simulations will cover more complex multicomponent mixtures and a wider particle size range. (***shown in lines 648 ~ 654 , page 36 in the revised manuscript***)

5. **Have the authors performed any size-dependence analysis to ensure that the reported contact angles are not artifacts of finite droplet size?**

Answer: Thank you for this important comment. We varied water-molecule counts (8000–32000) at fixed dodecane number to generate droplets of different sizes (< 20 nm), and the size-related contact angle trend is shown in Figure 3. However, changing water content modifies both droplet dimension and water-dodecane ratio, so pure size-dependence at fixed composition cannot be fully isolated.

We mitigated finite-size artefacts via Tolman-length curvature correction for interfacial tension and the line-tension-modified Young's equation. Strict fixed-composition size-scaling simulations require proportional scaling of all species, which is computationally prohibitive and beyond this work's scope. Our quantitative results apply only for droplets < 20 nm. We have added this limitation to the revised manuscript.

It should be acknowledged that our model systems are simplified compared to real multi-organic multi-salt atmospheric aerosols. All simulated LLPS droplets are smaller than 20 nm, representative of fresh nucleation mode ultrafine particles from new particle formation and fuel combustion. Though these nanoparticles dominate ambient aerosol number concentrations and govern early aging processes, our results cannot be directly extrapolated to larger aged accumulation mode aerosols. Future simulations will cover more complex multicomponent mixtures and a wider particle size range. (***shown in lines 648 ~ 654 , page 36 in the revised manuscript***)

6. **How was equilibrium verified? Were longer simulations performed to confirm that the contact angle had fully converged?**

Answer: Thank you very much for this valuable comment. In this study, The interaction energy between water molecular clusters and dodecane clusters ($E_{w\text{-}d}$) were monitored to determine if the simulation had reached equilibrium. In the revised manuscript, as a representative, temporal evolutions of $E_{w\text{-}d}$ in the LLPS droplet consisted of 2000 dodecane and 8000 water at the temperature of 280 K are present. Correspondingly, the

temporal evolutions sphericity metric (S_{fit}) of the water (dodecane) cluster and the contact angle in the 2000 dodecane – 8000 water system at T = 280 K are included. The added contents are listed below.

The interaction energy between water molecular clusters and dodecane clusters ($E_{w\text{-}d}$) were monitored to determine if the simulation had reached equilibrium. As a representative, Fig. S2 presents temporal evolutions of $E_{w\text{-}d}$ in the LLPS droplet consisted of 2000 dodecane and 8000 water at the temperature of 280 K. Correspondingly, the temporal evolutions sphericity metric (S_{fit}) of the water (dodecane) cluster and the contact angle in the 2000 dodecane – 8000 water system at T = 280 K are shown in Fig. S3-S4. It can be observed that $E_{w\text{-}d}$ approximately reaches equilibrium after 8 ns, and accordingly, the S_{fit} of both clusters and the contact angle approximately stabilize.

(*shown in lines 130 ~ 138 , pages 6-7 in the revised manuscript*)

Fig. S2 presents an example of energy-tracking analysis, recording the time-evolution of interaction energy between water molecular clusters and dodecane clusters ($E_{w\text{-}d}$) for the 2000 dodecane – 8000 water system at 280 K based on the OPLS-UA force field. The system is considered to have attained equilibrium once the energy profile converges to an approximate stable value. Following equilibration, atomic-position trajectories were sampled statistically every 2 ps over a total simulation duration of 3 ns.

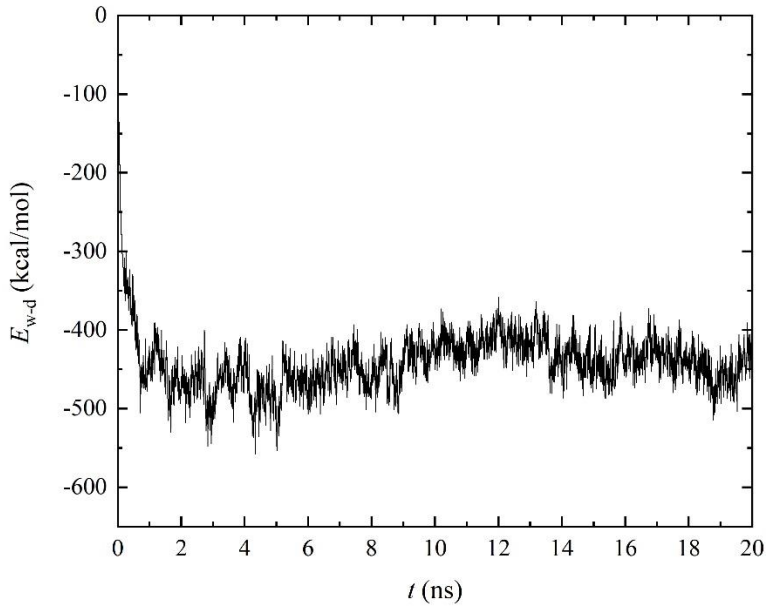


Fig. S2 The interaction energy between the water cluster and the dodecane cluster ($E_{w\text{-}d}$) in the LLPS droplet consisted of 2000 dodecane and 8000 water at the temperature of 280 K, and the MD simulation is based on the OPLS-UA force field

The sphericity metric of the droplet (S_{fit}) is quantified based on the residual error from density profile fitting, consistent with the interface detection workflow adopted for contact angle calculation in this work. S_{fit} is given by

$$S_{fit} = 1 - \frac{\delta_{RMS}}{R_{fit}} \tag{3}$$

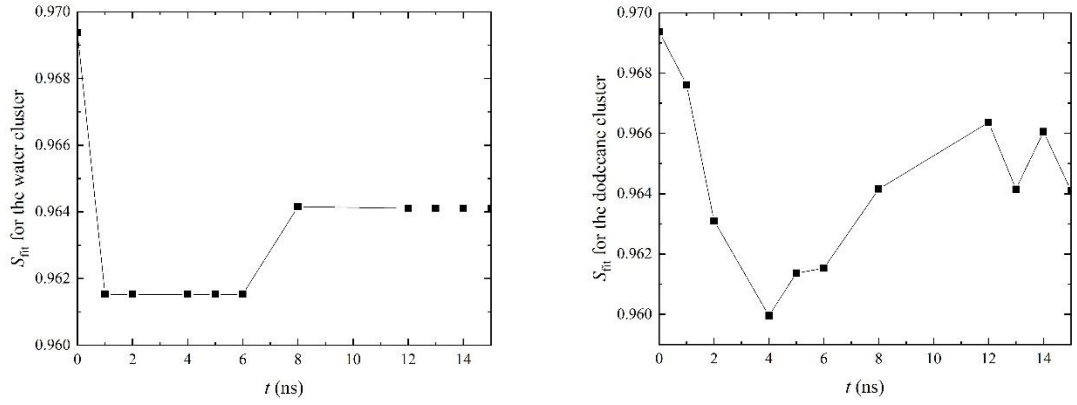
where δ_{RMS} is the Root mean square deviation of the distance from the interface point to the fitted sphere. R_{fit} is the optimal sphere radius obtained by least squares fitting. The δ_{RMS} is calculated by

$$\delta_{RMS} = \sqrt{\frac{1}{N_j}\sum\nolimits_j (R_j - R_{fit})^2} \tag{4}$$

where R_j is the distance from each interface point to the centroid.

The temporal evolutions of S_{fit} for the water cluster and the dodecane cluster in the 2000 dodecane – 8000 water system at T = 280 K have been calculated, and the results are shown in Fig. S3. It can be easily found that the sphericity decreases first and then increases as the simulation progresses. At the initial stage, water clusters and dodecane clusters are ideal spherical shapes directly generated by software, therefore their

sphericity is relatively high. With the evolution of the simulation, structural relaxation of the two clusters causes an initial reduction and subsequent rise in sphericity, with both clusters attaining near-equilibrium at approximately 8 ns. At equilibrium, the sphericity of both clusters is greater than 0.963, which proves the reliability of the assumption of spherical caps in calculating contact angles. At equilibrium, the sphericity of both clusters is greater than 0.963, which proves the reliability of the assumption of cluster sphericity in calculating contact angles.



(a) (b)

Fig. S3 Temporal evolutions of S_{fit} for the water cluster (a) and the dodecane cluster (b) in the 2000 dodecane – 8000 water system at T = 280 K

The time evolution of the contact angle in the 2000 dodecane – 8000 water system at T = 280 K is shown in Fig. S4

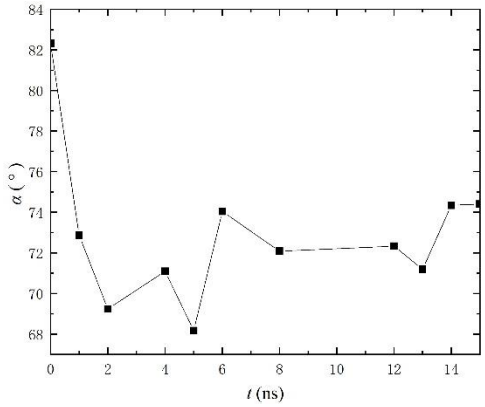


Fig. S4 Temporal evolution of the contact angle in the 2000 dodecane – 8000 water system at T = 280 K

(*shown in lines 71 ~ 111 , pages 4-6 in the Supplement file*)

7. **Can the authors provide statistical uncertainties or confidence intervals for the calculated contact angles and line tensions?**

Answer: We appreciate the reviewer's valuable comment.

For the liquid-liquid contact angles, statistical uncertainties are already represented by error bars shown in Figure 3, Figure 5 and Figure 7 in the main manuscript. These error bars denote the standard deviation (SD) obtained from independent replicate MD simulation runs for each condition, where each system was simulated three times under identical setup, and snapshots were sampled over the equilibrium production trajectory for statistical averaging.

For line tension, which is a derived quantity calculated from contact angle and multiple interfacial-tension inputs via the modified Young's equation (Eq. 8), its statistical uncertainty propagates from the uncertainties of contact angle and interfacial tension. Directly plotting error bars for line-tension data in Figure 10 would lead to highly cluttered figures due to error propagation amplification. Instead, we have added detailed description in the revised manuscript text to explicitly state the source of statistical uncertainty for line tension: the uncertainties originate from the standard deviations of contact-angle and interfacial-tension outputs from repeated MD replicates. The fitted quartic-polynomial parameters for line tension (Table S8 in supplement) are obtained from the mean values of line-tension datasets under each temperature.

The uncertainties of line tensions originate from the standard deviations of contact angle and interfacial tension outputs from repeated MD replicates. The fitted quartic-polynomial parameters for line tension are obtained from the mean values of line-tension datasets under each temperature.

(***shown in lines 470 ~ 474 , page 26 in the revised manuscript***)

8. **Why was a fourth-order polynomial selected? Was this based on physical reasoning or simply because it gave the smallest fitting error?**

Answer: Thanks for this important comment.

No fundamental physical formula exists to analytically describe how line tension varies with temperature for liquid-liquid-vapor contact lines in nanoscale LLPS aerosols. We compared polynomial fits of different orders. Lower-order polynomials (1–3 order) cannot reproduce the non-monotonic trends of MD-calculated line tension and show large fitting residuals. Higher-order polynomials (>4th-order) risk over-fitting and spurious unphysical oscillations.

The fourth-order polynomial is selected as an empirical compromise between fitting quality and over-fitting prevention. It is only valid for interpolation within our simulated temperature range (240–320 K), and should not be used for extrapolation. This limitation has been added to the revised manuscript:

Note that there is currently no analytical function describing the temperature dependence of line tension for nanoscale liquid-liquid-vapor contact lines. Polynomials of lower orders (1st-3rd) were tested but exhibited large residuals and failed to capture the non-monotonic variations observed in MD outputs. Higher-order polynomials (>4th-order) were avoided to prevent over-fitting and artificial oscillations. The resulting quartic fit serves purely as an empirical interpolation tool valid within our simulated temperature range (240 (280)–320 K), while extrapolation beyond this range is not physically justified.

(shown in lines 474 ~ 481 , pages 26-27 in the revised manuscript)

9. Can the authors provide a molecular interpretation of why increasing temperature consistently increases the contact angle?

Answer: We appreciate this insightful question. The contact angle increases with temperature mainly due to the differential temperature responses of three interfacial tensions (γ_{wv}), (γ_{ov}), (γ_{wo}). Higher temperature enhances molecular thermal motion and weakens intermolecular cohesion at all interfaces, lowering all three interfacial tensions. For our liquid-liquid phase-separated nanodroplets, the temperature-driven decrease of

(γ_{wv} - γ_{ov}) is larger in magnitude than the decrease of (γ_{wo}). From the interfacial energy balance (cos α'= (γ_{wv} - γ_{ov})/γ_{wo}), this yields a larger contact angle at elevated temperature. At the molecular scale, the elevated thermal fluctuations disrupt water-water hydrogen-bond networks at the water surface, which produces a large reduction in water-vapor interfacial tension (γ_{wv}) as temperature rises. For γ_{ov}, intermolecular interactions are weak van-der-Waals forces between alkane chains, and the reduction of γ_{ov} caused by the increasing temperature is smaller than for γ_{wv}. Consequently, γ_{wv} - γ_{ov} decreases appreciably with increasing temperature. The water-dodecane liquid-liquid interface is characterized by the unfavourable contact between hydrogen-bonded water and non-polar dodecane. Thermal agitation perturbs interfacial molecular packing and reduces this excess free energy, so γ_{wo} also falls with temperature. However, its fractional reduction is less pronounced than for γ_{wv} - γ_{ov}.

The revisions incorporated in the revised manuscript are listed below.

At the molecular scale, heating strongly disrupts hydrogen-bond networks at the water-vapor interface and reduces γ_{wv} substantially, while the reduction of van-der-Waals-dominated γ_{ov} and water-dodecane γ_{wo} are comparatively weaker. Line tension further modifies absolute contact-angle values but does not reverse this positive temperature trend.

(***shown in lines 519 ~ 523 , page 29 in the revised manuscript***)

10. Is the NaCl aggregation observed with Martini a physical prediction or a known artifact of the coarse-grained force field?

Answer: Thank you for this important question. The NaCl-induced aqueous-cluster deformation seen at high salt in Martini simulations is an inherent coarse graining artifact of the Martini force field, supported by the lack of equivalent aggregation in identical OPLS-UA simulations. This artifact can be ignored at low NaCl concentrations. Contact angle results based on the Martini force field values at high NaCl must therefore be interpreted cautiously, as part of the observed contact angle

reduction arises from artefact of the Martini force field rather than purely interfacial thermodynamics.

The Martini force field has inherent flaws in describing the interface phenomena of aqueous droplets, but it is widely used in qualitative research due to its advantage in computational complexity. We discussed it in the revised manuscript.

The Martini force field parameters have limitations in describing the surface tension of pure water and therefore the water-dodecane contact angle. The core problem of the Martini force field lies in the compromises inherent in its coarse-grained design: representing multiple water molecules with a single bead eliminates orientational degrees of freedom and hydrogen-bond directionality, yet water's surface tension arises precisely from the anisotropic net attraction caused by surface molecules being unable to form a complete hydrogen-bonding network. Meanwhile, in Martini force field each water bead is modeled as a simple 12-6 Lennard-Jones particle, and its nonbonded parameters are optimized for bulk-phase partitioning free energies. Because such a simplified LJ potential is known to overly stabilize the solid phase and cause unphysical freezing at elevated temperatures, the force field deliberately avoids using surface tension as a fitting target. Consequently, its water beads lack explicit hydrogen bonding and electrostatics, causing the predicted surface tension of pure water to be only about one-third of the experimental value (Iannetti et al., 2024). Nevertheless, despite these limitations in quantitatively reproducing interfacial properties, The Martini force field remains a highly efficient coarse-grained model, valuable for investigating qualitative mechanisms underlying how microscopic parameters modulate interfacial behavior, especially for exploring particle size effects.

(***shown in lines 601 ~ 618 , page 34 in the revised manuscript***)

11. At approximately what droplet size does the line-tension correction become negligible so that the classical Young equation becomes valid?

Answer: Thank you for this important question. According to the theoretical work of Qiu and Molinero (2015) on liquid-liquid phase-separated aerosols, the classical Young

equation becomes approximately valid for LLPS aerosol particles with total diameter larger than ~100 nm, where line-tension contributions can be safely neglected. For ultrafine particles below ~100 nm, line tension exerts a non-negligible influence on apparent liquid-liquid contact angles, which is consistent with our present MD results: all droplets in our simulations are smaller than 20 nm and show clear deviations between MD-derived contact angles and Young-equation predictions.

Our current MD simulations only cover droplets < 20 nm, so we cannot directly determine the crossover size from our own simulation dataset. Besides, the threshold size of ~100 nm is an approximate reference value for water-alkane type LLPS systems. The exact crossover size still depends on the magnitude and sign of line tension, which varies with chemical composition and temperature. Therefore, systematic simulations across broader particle-size ranges would be required to quantitatively refine this threshold for various typical systems in future work.

The revisions incorporated in the revised manuscript are listed below.

According to Qiu and Molinero (2015), line-tension corrections become negligible and classical Young's equation is approximately valid for LLPS aerosol particles with diameter > ~100 nm. All droplets in our MD work are below 20 nm, hence large deviations from Young's equation are observed. This crossover size is approximate and composition-dependent, because line-tension magnitude and sign change with temperature and composition. Further simulations covering wider particle-size ranges would help refine this threshold for various typical systems.

(***shown in lines 594 ~ 600 , pages 33-34 in the revised manuscript***)

12. How sensitive are the calculated contact angles to the fitting procedure and the bin size used to determine the droplet interface?

Answer: Thank you for this important question. We investigated the sensitivity toward bin-size by re-processing identical MD trajectories without changing simulation parameters or fitting workflow. Five cylindrical bin heights Δz = 2.0 Å, 2.5 Å, 3.0 Å, 4.0 Å, and 5.0 Å were tested on representative 2000 dodecane – 8000 water LLPS

droplet system (T = 280 K), and the results are presented in the following Fig. S5.

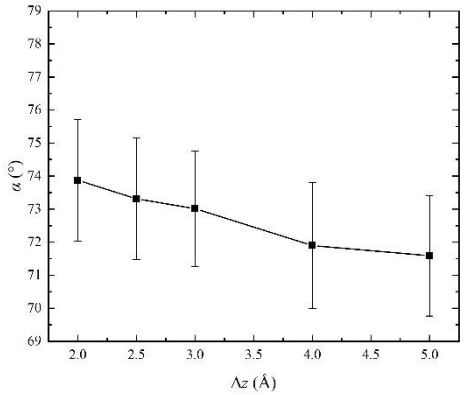


Fig. S5 Effect of cylindrical bin heights (Δz) on the calculated contact angle (α) in the 2000 dodecane – 8000 water LLPS droplet system (T = 280 K)

It can be observed from Fig. S5 that with Δz decreases from 5.0 Å to 2.0 Å α increases slowly. At Δz = 2.0-3.0 Å, contact angle differences induced by varying Δz remain below ±2.5°, which falls within the statistical error bars. Reducing the length will increase the computational complexity, therefore, after considering both the computational complexity and accuracy, we set the length to 2.5 Å.

The reliability of the fitting procedure can be further quantified by the sphericity metric $S_{fit} = 1 - \delta_{RMS}/R_{fit}$, where δ_{RMS} is the root-mean-square deviation of the interface points from the least-squares fitted sphere. For the LLPS droplet system consisting of 2000 dodecane and 8000 water molecules at T = 280 K, the fitted spherical parameter S_{fit} exceeds 0.963 for both water and dodecane clusters at equilibrium (Fig. S3). This gives $\delta_{RMS}/R_{fit} < 0.037$, meaning the interfacial points deviate from the fitted sphere by less than 3.7% of the fitted radius. This result verifies the robustness of the least-squares fitting and validates the self-consistency of the spherical-cap assumption adopted in Eq. (1).

The revisions incorporated in the revised manuscript are listed below.

2. Sensitivity of contact angle to cylindrical bin height

To investigated the calculated contact angle (α) to the cylindrical bin height (Δz), five cylindrical bin heights Δz = 2.0 Å, 2.5 Å, 3.0 Å, 4.0 Å, and 5.0 Å were tested on representative 2000 dodecane – 8000 water LLPS droplet system (T = 280 K), and the

results are presented in the following Fig. S5.

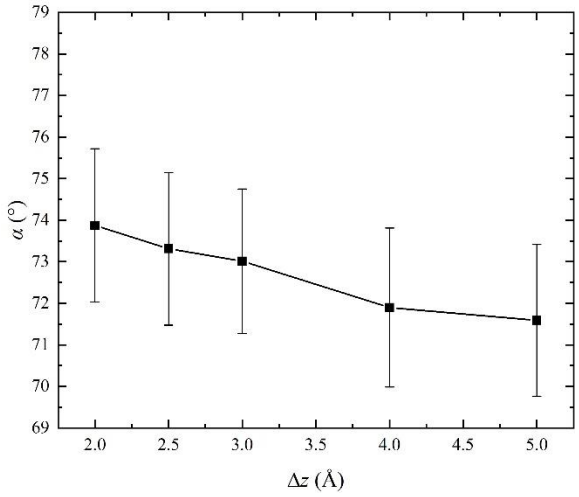


Fig. S5 Effect of cylindrical bin heights (Δz) on the calculated contact angle (α) in the 2000 dodecane – 8000 water LLPS droplet system (T = 280 K)

It can be observed from Fig. S5 that with Δz decreases from 5.0 Å to 2.0 Å α increases slowly. At Δz = 2.0-3.0 Å, differences between average contact angles induced by varying Δz remain below 0.9°, which falls within the statistical error bars. Reducing the length will increase the computational complexity, therefore, after considering both the computational complexity and accuracy, we set the length to 2.5 Å.

(shown in lines 128~ 140 , page 9 in the supplement file)

The sphericity metric of the droplet (S_{fit}) is quantified based on the residual error from density profile fitting, consistent with the interface detection workflow adopted for contact angle calculation in this work. S_{fit} is given by

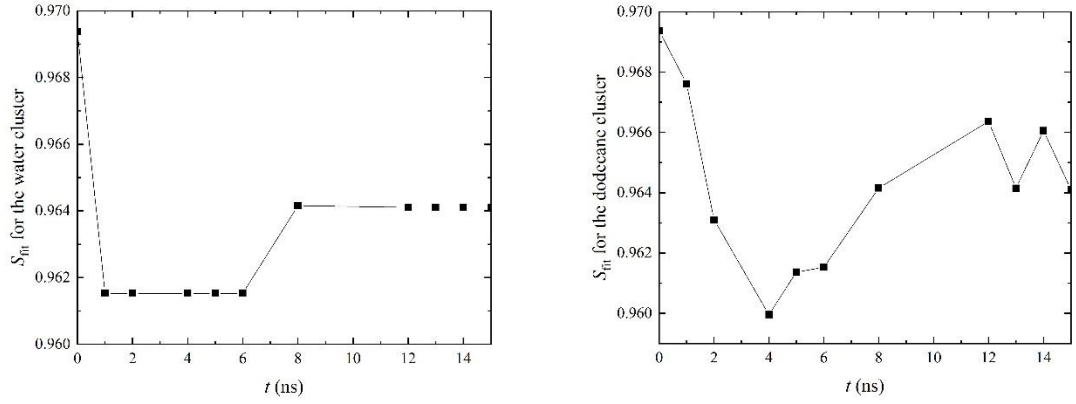
$$S_{fit} = 1 - \frac{\delta_{RMS}}{R_{fit}} \tag{3}$$

where δ_{RMS} is the Root mean square deviation of the distance from the interface point to the fitted sphere. R_{fit} is the optimal sphere radius obtained by least squares fitting. The δ_{RMS} is calculated by

$$\delta_{RMS} = \sqrt{\frac{1}{N_j}\sum_j (R_j - R_{fit})^2} \tag{4}$$

where R_j is the distance from each interface point to the centroid.

The temporal evolutions of S_{fit} for the water cluster and the dodecane cluster in the 2000 dodecane – 8000 water system at T = 280 K have been calculated, and the results are shown in Fig. S3. It can be easily found that the sphericity decreases first and then increases as the simulation progresses. At the initial stage, water clusters and dodecane clusters are ideal spherical shapes directly generated by software, therefore their sphericity is relatively high. With the evolution of the simulation, structural relaxation of the two clusters causes an initial reduction and subsequent rise in sphericity, with both clusters attaining near-equilibrium at approximately 8 ns. At equilibrium, the sphericity of both clusters is greater than 0.963, which proves the reliability of the assumption of spherical caps in calculating contact angles. At equilibrium, the sphericity of both clusters is greater than 0.963, which proves the reliability of the assumption of cluster sphericity in calculating contact angles.



(b) (b)

Fig. S3 Temporal evolutions of S_{fit} for the water cluster (a) and the dodecane cluster (b) in the 2000 dodecane – 8000 water system at T = 280 K

(shown in lines 82 ~ 106 , pages 4-5 in the supplement file)

13. Can the authors estimate how much including line-tension corrections would change predictions of aerosol morphology in existing climate or atmospheric chemistry models?

Answer: Thank you for this thoughtful question. To our knowledge, current

climate-atmospheric chemistry models do not explicitly implement line-tension corrections for liquid-liquid phase-separated aerosol morphology. These models mostly adopt macroscopic Young-equation-based contact-angle or fixed-morphology assumptions (core-shell / fully-mixed), without nanoscale line-tension terms.

As reported in our manuscript and consistent with Qiu and Molinero (2015), line-tension corrections become substantial for ultrafine LLPS droplets below ~100 nm diameter, while its influence diminishes and can be safely neglected for particles larger than this approximate threshold. All our MD simulations are performed for droplets < 20 nm; our fitted quartic-polynomial line-tension parametrization is only validated within our simulated temperature-composition window and cannot be directly extrapolated to the broader size/composition range required by global models. Therefore, we cannot provide a robust quantitative estimate for global-model morphology shifts at this stage.

Qualitatively, for ultrafine nanosized LLPS aerosols (< 100 nm), ignoring line tension will bias contact-angle predictions, which further alters the predicted partial-wetting / engulfment morphology, the interfacial contact area between two liquid phases, and the effective surface-area-weighted surface tension. For accumulation-mode particles (> 100 nm), morphology predictions from classical Young's equation would have little difference whether line-tension is included or not.

We have added a short clarifying paragraph in the discussion section of revised manuscript to state the above limitation: our line-tension results are derived for sub-20 nm model droplets; direct implementation into large-scale atmospheric models requires further work covering wider particle sizes and real-world multicomponent aerosol systems. Future work could upscale MD-derived line-tension data toward usable parameterizations for aerosol modules in climate models.

Furthermore, to enhance the atmospheric environmental significance of this study, effects of contact angle on the saturated vapor pressure of water on the surface of a droplet and the condensation rate of water on the surface of the droplet have been added in the revised manuscript.

The revisions incorporated in the revised manuscript are listed below.

To provide quantitative evidence, the water vapor supersaturations SS/[100%] = *S*-1 of droplet composed of 8000 water, 2000 dodecane and 100 NaCl at various temperatures (280, 290, 300, 310, 320 K) have been calculated by Köhler theory using E-AIM-derived water activities and three different description methods of surface tension. In Method 1, the droplet surface tension is calculated based on the surface-area-weighted mean of the surface tensions from NaCl solution phase and dodecane phase together with the contact angle reported in Fig. 5(b). In Method 2, surface tension of the NaCl solution droplet derived from E-AIM model is used. In Method 3, it is assumed that dodecane completely envelops the sodium chloride solution droplet in shell form, and the surface tension of the droplet is equal to that of squalane. Comparison of *SS* and the corresponding surface tension are presented in Fig. 11. It can be observed from Fig. 11(a) that at all temperatures the results of *SS* using different methods satisfy the following order: Method 2 > Method 1 > Method 3. It can be explained by the consistent order of droplet surface tension shown in Fig. 11(b).

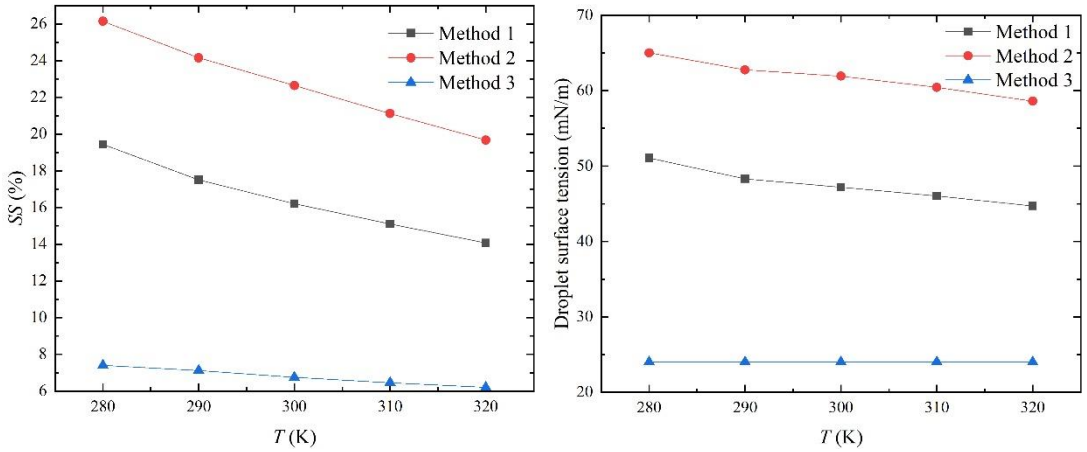


Fig. 11 Comparison of *SS* of 8000 water - 2000 dodecane - 100 NaCl droplet at various temperatures (280, 290, 300, 310, 320 K) calculated based on three different description methods of surface tension (a) and the corresponding surface tension (b)

The heat and mass accommodation coefficients are key parameters in the theoretical model of heat and mass transfer at gas-liquid interface (Zhang et al., 2025; Shiraiwa et al., 2010; Nguyen et al., 2026), but they cannot be measured directly. In

many existing studies, heat and mass accommodation coefficients are always set to 1 or a fixed empirical value, which may be unreasonable.

If the adsorption coefficient of each liquid phase in the liquid-liquid phase separation particles is known, the equivalent accommodation coefficients can be obtained based on the surface-area-weighted mean which can be calculated by the contact angle. A case study was implemented to compare the effects of different surface accommodation coefficients on droplet condensation process. The condensation rates of the droplet composed of 8000 water, 2000 dodecane and 100 NaCl at various temperatures (280, 290, 300, 310, 320 K) under a water vapor saturation of $S = 1.6$ were calculated based on the Kumala model (Kulmala et al., 1993) with two different mass (heat) accommodation coefficients (λ_M and λ_T). In the first scenario, both mass and heat accommodation coefficients were calculated using the corresponding contact angle (Fig. 5(b)) (Model S1), while they are set to 1 in the second scenario (Model S2). Details of the Kumala model are presented in the Supplement. The condensation rates (dr/dt) and the mass (heat) accommodation coefficients (λ_M and λ_T) at the initial time based on two models are presented in Fig. 12.

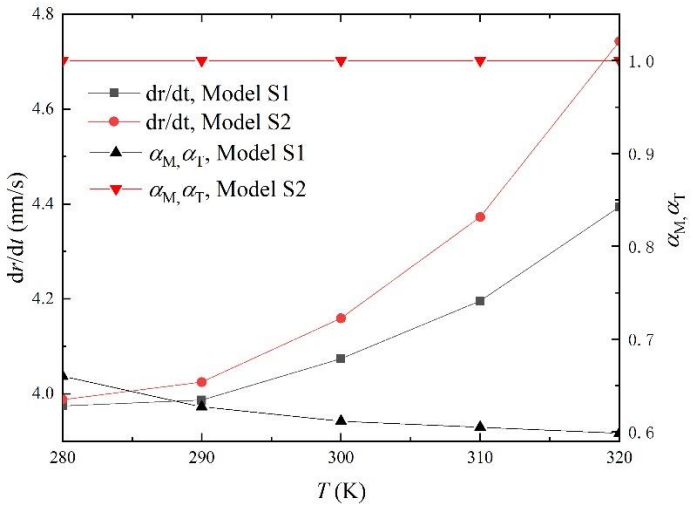


Fig. 12 The theoretical condensation rates (dr/dt) the mass (heat) accommodation coefficients (λ_M and λ_T) at the initial time of the droplet composed of 8000 water, 2000 dodecane and 100 NaCl at various temperatures (280, 290, 300, 310, 320 K) under a water vapor saturation of $S = 1.6$

As shown in Fig. 12, compared with Model 2, calculating the mass (heat)

accommodation coefficients from the contact angle leads to a considerable reduction in droplet condensation rate. This study provides ideas for the quantitative description of contact angle, and in the future, the calculation method of contact angle can be improved through the study of LLPS particles with various components and sizes.

(***shown in lines 546 ~593 , pages 30-33 in the revised manuscript***)

References

Iannetti, L., Cambiaso, S., and Rasera, D. T., Antonio: The surface tension of Martini 3 water mixtures, J. Chem. Phys., 161, 2024.

Jorgensen, W. L., Maxwell, D. S., and Tirado-Rives, J.: Development and testing of the OPLS all-atom force field on conformational energetics and properties of organic liquids, J. Am. Chem. Soc., 118, 11225-11236, 1996.

Kulmala, M., Vesala, T., and Wagner, P. E.: An analytical expression for the rate of binary condensational particle growth, Proceedings of the Royal Society of London. Series A: Mathematical and Physical Sciences, 589-605, 1993.

Nguyen, K., Schervish, M., Lakey, P. S., Smith, J. N., and Shiraiwa, M.: Impact of particle phase state on the competition between condensation and coagulation, Environ. Sci.-Atmos., 2026.

Obeidat, A., Hrahsheh, F., and Wilemski, G.: Scattering Form Factors for Russian Doll Aerosol Droplet Models, J. Phys. Chem. B, 119, 9304-9311, 2015.

Shiraiwa, M., Pfrang, C., and PöSchl, U.: Kinetic multi-layer model of aerosol surface and bulk chemistry (KM-SUB): the influence of interfacial transport and bulk diffusion on the oxidation of oleic acid by ozone, Atmos. Chem. Phys., 10, 367-373, 2010.

Zhang, C., Lu, M., Bao, H., Ma, N., Yu, D., Yang, Y., Wang, Y., and Wiedensohler, A.: An improved model on the evaporation kinetics of the single aerosol droplet and its application for the droplet composed of ammonium sulfate or sucrose solution, Powder Technol., 120627, 2025.